# Molecular dynamics study of melting of the bcc metal vanadium. II. Thermodynamic melting

V. Sorkin,* E. Polturak, and Joan Adler

*Physics Department, Technion–Israel Institute of Technology, Haifa 32000, Israel*

We present molecular dynamics simulations of the thermodynamic melting transition of a bcc metal, vanadium, using the Finnis-Sinclair potential. Our motivation was to answer the question whether premelting phenomena, extensively studied for fcc metals, are also present in bcc metals. We studied the structural, transport, and energetic properties of slabs made of 27 atomic layers with a free surface. We investigated premelting phenomena at the low-index surfaces of vanadium, V(111), V(001), and V(011), finding that as the temperature increases, the V(111) surface disorders first, then the V(100) surface, while the V(110) surface remains stable up to the melting temperature. Also, as the temperature increases, the disorder spreads from the surface layer into the bulk, establishing a thin quasiliquid film in the surface region. We conclude that the hierarchy of premelting phenomena is inversely proportional to the surface atomic density, being most pronounced for the V(111) surface which has the lowest surface density.

## I. INTRODUCTION

Theories of melting[1,2,4] can be separated into two classes. The first one describes the *mechanical melting* of a homogeneous solid resulting from lattice instability[5-7] and/or the spontaneous generation of thermal defects.[8-11] The second class treats the *thermodynamic melting* of heterogeneous solids, which begins at extrinsic defects such as a free surface or an internal interface (grain boundaries, voids, etc.).[3,12-18] Both types of melting have been studied extensively for the case of fcc metals. In order to determine whether the mechanism of homogeneous melting differs if the lattice symmetry is changed, in our first paper,[19] we extended these studies to a bcc metal, vanadium. We used molecular dynamics simulations to study the mechanical melting transition in a bulk system and found that the melting transition occurs uniformly throughout the solid at the melting point. The shear elastic instability leading to this melting of vanadium occurred once the molar volume reached a critical value, whether reached by heating the solid or by adding defects at a constant temperature.[19] The temperature at which the mechanical melting transition takes place in our model is $T_s = 2500 \pm 10$ K, which is above the melting temperature measured experimentally, $T_m = 2183$ K. Thus, the mechanical melting transition can be observed only if melting at surfaces is artificially suppressed, since in the laboratory it is preempted by the thermodynamic melting transition which begins at a free surface. This paper is devoted to a comparison of the thermodynamic melting of bcc metals which were not previously investigated, with fcc metals which were extensively researched both theoretically and experimentally.

Theoretical aspects of melting beginning at the surface have been studied by phenomenological theories,[15,20-22] lattice-gas models,[16] and density functional theory.[23] Microscopic descriptions of static and dynamic properties of melting phenomena beginning at a surface emerged from computer simulations which employ many-body interaction potentials derived from the effective-medium[24-26] and embedded-atom theories,[17,27-30] as well as pairwise interatomic interactions in the form of Lennard-Jones

potentials.[31,32] Melting at the surface is anisotropic, meaning that certain surfaces of fcc metals [Pb(110), Al(110)] exhibit premelting,[15] while this phenomenon is not observed for close-packed surfaces [Pb(111), Al(111)]. Theoretical aspects of this anisotropy were discussed by Trayanov and Tosatti.[16]

This paper is organized as follows: details of the molecular dynamics simulations are presented in Sec. II. Section III contains most of the results of this study, including the thermodynamic melting temperature and several structural, energetic, and transport properties of the surface. Finally, in Sec. IV, we summarize our results.

## II. SIMULATION DETAILS

We model the melting of vanadium with a free surface using molecular dynamics (MD) simulations[33,34] in a canonical ensemble. The many-body interaction potential used in this study was developed by Finnis and Sinclair[35] (FS). The computational aspects of the algorithm are described in detail in our previous article.[19]

Ideally, a crystal with a surface is a semi-infinite system. We modeled this system as a thick slab. This slab is shown in Fig. 1. The bottom 3 atomic layers have the positions of atoms fixed in order to mimic the effect of the presence of the infinite bulk of the crystal. Due to the relatively short range of the repulsive part of the modified FS potential, 3 fixed layers are sufficient to represent the static substrate. On top of those 3 layers there are 24 layers in which the atoms are free to move. We have also used samples with 17 and 20 free layers. We found that the surface properties discussed in the following were less sensitive to the substrate as the number of free layers increased. With 24 layers, the influence of the substrate was within the noise of the simulations. Periodic boundary conditions are used along the in-plane ($x$ and $y$) directions, while the top boundary of the slab, along the $z$ direction, is free. In Fig. 1 we show a sample where the temperature is high enough ($T = 2100$ K) so that the layers near the free surface are already disordered.

Three different samples with various low-index surfaces were constructed: V(001), V(011), and V(111), whose sur-
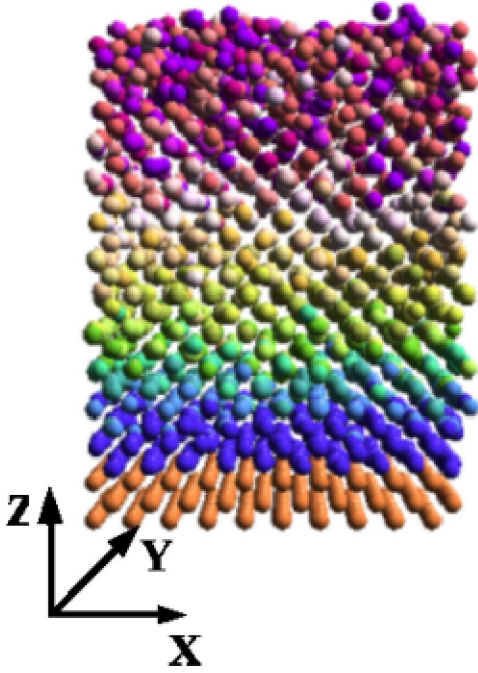
FIG. 1. (Color online) Geometry of the sample V(001) surface.

face layers are shown in Fig. 2. The V(001) and V(111) samples contain 2700 atoms, initially arranged as a perfect bcc crystal of $10 \times 10 \times 27$ unit cells (100 atoms in a layer). The V(011) sample contains 2646 atoms arranged as $7 \times 7 \times 27$ unit cells (98 atoms in a layer).

Each simulation starts from a low-temperature solid. The lattice constant of the frozen layers is assigned a value appropriate to the bulk.[19] As the temperature is raised, this value is adjusted to reflect thermal expansion as obtained from bulk simulations.[19] We found that $\sim 10^5$ integration time steps were sufficient in order to reach thermal equilibrium after a temperature change (a time step $dt = 1.05 \times 10^{-15}$ s). An equilibrium state is considered to be achieved when there is no significant temporal variation (beyond the statistical fluctuations) of the total energy, layer occupation number, structure order parameters, self diffusion coefficients, and a uniform profile of kinetic temperature across the sample is observed. Thereafter the various structural and transport properties of the system are calculated, accumulated, and averaged over a long period of $10^7$ MD steps. Throughout this study, interactive visualization (the AVIZ program[36]) was implemented to observe sample disorder and layer mixing (see Fig. 1). A discussion of this visualization can be found in Ref. 37.
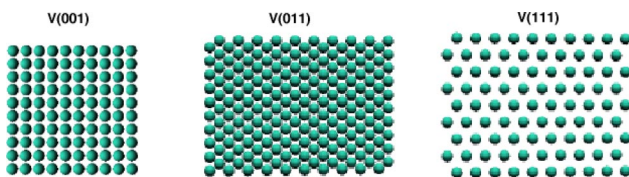


FIG. 2. Geometry of the low-index faces of vanadium (top view). The drawings are to scale.

## III. PREMELTING EFFECTS ON SURFACES

### A. Thermodynamic melting temperature

In order to investigate the phenomenon of surface disorder and premelting, we first determined the thermodynamic melting point $T_m$ of vanadium described by the modified FS potential. $T_m$ was obtained by means of the method proposed by Lutsko *et al.*[38] In this method one raises the temperature of the solid abruptly to $T_0$, well above $T_m$, and creates a solid-melt interface. The interface propagates from the surface inward. The value of $T_m$ is not known, but the speed of the interface is proportional to $T_0 - T_m$. Consequently, the melting temperature can be found as the value of $T_0$ at which solid-melt interface becomes stationary (coexistence).

In this way, we found $T_m = 2220 \pm 10$ K for the V(111) sample, which has the lowest surface packing density. This value is close to the experimental value[39] of $T_m = 2183$ K. For the other surfaces, the value of $T_m$ comes out slightly higher, but within the uncertainty limits of the simulation. The difference could be due to superheating effects on the solid-liquid interface just above the thermodynamical melting point $T_m$. The largest difference is found for the close-packed V(011) surface, with $T_m \approx 2240 \pm 10$ K. This dependence of the thermodynamic melting point on the crystalline plane forming the surface was also observed in MD simulations of fcc metals.[11,24,26–28]

### B. Surface thermal expansion and amplitude of atomic vibration

The interlayer relaxation and surface thermal expansion was calculated using the difference between the average $z$ coordinate of the $i$th and $i+1$th layers:

$$d_{i,i+1} = \left\langle \frac{1}{n_{i+1}} \sum_{j \in i+1} z_j - \frac{1}{n_i} \sum_{j \in i} z_j \right\rangle, \qquad (1)$$

where $z_i$ is the $z$ coordinate of the atom $i$, $n_i$ is the instantaneous number of atoms in the layer $i$, and the angular brackets denote a time average. The distances between the neighboring layers could be determined up to temperatures where surface premelting effects blur the distinction between individual layers, although some structure remains visible in the local density profiles (see below).

At low temperatures, the first layer exhibits an inward relaxation, i.e., $\Delta_{1,2} < 0$, where we define

$$\Delta_{i,i+1} = \frac{d_{i,i+1} - d_{bulk}}{d_{bulk}}, \qquad (2)$$

where $d_{i,i+1}$ is the distance in the $z$ direction between the $i$ and $i+1$ surface layers, and $d_{bulk}$ is the distance between two neighboring layers in the bulk. In Figs. 3 and 4, $\Delta_{i,i+1}$ is plotted versus temperature for two of the low-index faces.

The effect of the different geometry of the various surfaces is reflected in the thermal expansion; i.e., a surface with a lower atomic density expands more than a surface which is close packed. As shown in Fig. 5, the thermal expansion of the V(111) surface layers is significantly larger than the thermal expansion of other surfaces and fixed layers
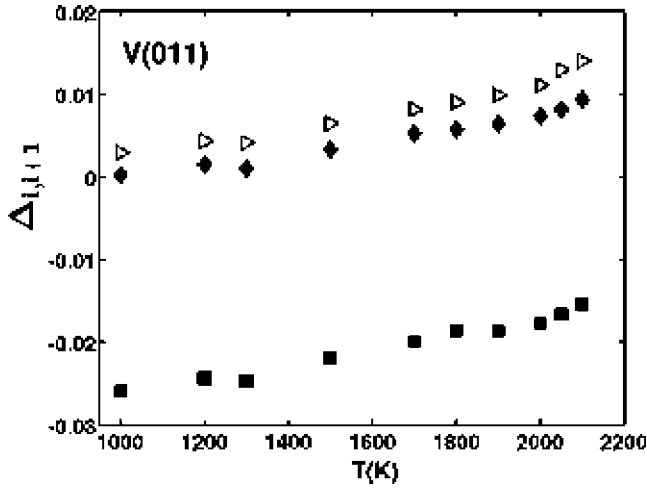
FIG. 3. Plot of $\Delta_{i,i+1}$ for the first (squares), second (triangles), and third (diamonds) surface layers as a function of temperature for the V(011) surface.

(bulk). In Fig. 6 we plot thermal expansion of surface layers [for the V(001) and V(011) slabs] and fixed layers on an enlarged scale. The observed "anomalous" thermal expansion of these surface layers is a direct consequence of enhanced vibration at the surface, where atoms probe the more anharmonic region of the interatomic potential. Anomalous thermal expansion was first observed in experiments on Pb(110) by Frenken and vander Veen.[14]

Atomic vibration properties at the different faces of vanadium are important for illustrating the onset of anharmonicity at high temperatures. We calculate the mean-square vibration amplitude (MSVA), $\langle u_\alpha^2 \rangle$ around the equilibrium position in the first surface layer as

$$\langle u_\alpha^2 \rangle = \frac{1}{n_1} \sum_{i=1}^{n_1} \langle [\vec{r}_{i,\alpha(t)} - \langle \vec{r}_{i,\alpha(t)} \rangle]^2 \rangle, \tag{3}$$
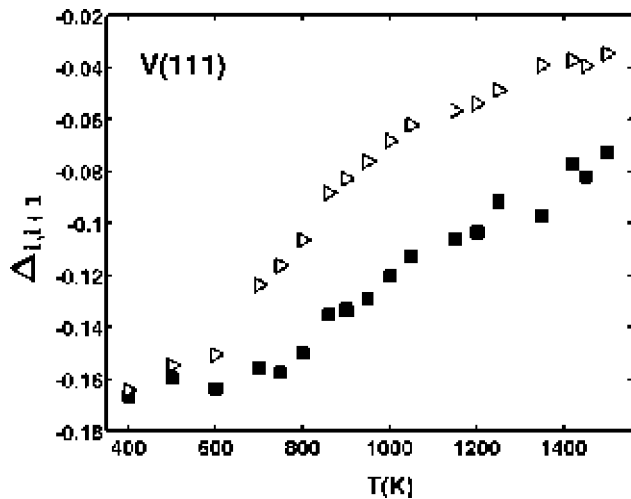


FIG. 4. Plot of $\Delta_{i,i+1}$ for the first (squares) and second (triangles) surface layers as a function of temperature for the V(111) surface.
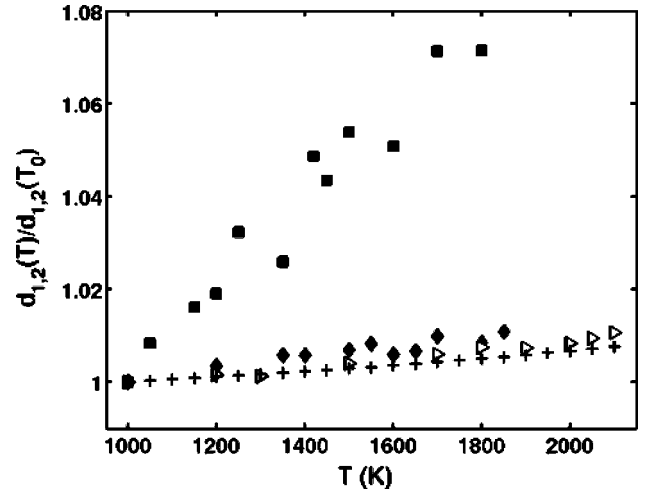
FIG. 5. Normalized interlayer distances between the first and second layers, $d_{1,2}(T)/d_{1,2}(T_0)$, at $T_0 = 1000$ K for the V(111) (squares), V(001) (diamonds), and V(011) (triangles) surfaces and the bulk (crosses). Note the anomalous thermal expansion of the V(111) surface.

where $\alpha = x, y, z$ denotes the spatial direction of motion, $n_1$ is the instantaneous number of atoms in the first surface layer, and the angular brackets represent an average over time.

In a harmonic system, $\langle u_\alpha^2 \rangle$ increases linearly with temperature, and therefore deviations from linearity are a measure of anharmonicity. The mean-square amplitudes of vibration shown in Fig. 7 for the V(111) surface demonstrate substantial anharmonicity at elevated temperatures. Figure 7 also shows that there is a noticeable difference between the in-plane MSVA $\langle u_x^2 \rangle$ and out-of-plane one $\langle u_z^2 \rangle$ (we found that $\langle u_x^2 \rangle \simeq \langle u_y^2 \rangle$). In-plane MSVA's are larger than out-of-plane amplitudes also for V(001) and V(011) surfaces. One reason for this anisotropy could be the different nearest-neighbor distances along the $x$ and $z$ directions caused by the inward relaxation of the surface layer, leading to a net restoring force that is higher in the direction perpendicular to the surface.
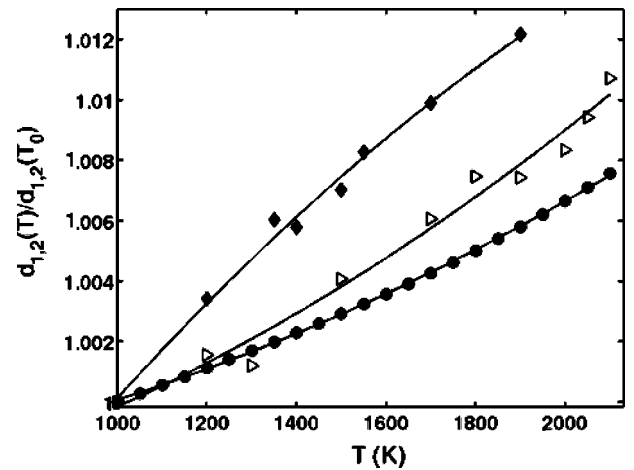


FIG. 6. Normalized interlayer distances between the first and second layers, $d_{1,2}(T)/d_{1,2}(T_0)$, at $T_0 = 1000$ K for the V(001) (diamonds) and V(011) (triangles) and the bulk (circles). The solid lines are drawn to guide the eye.
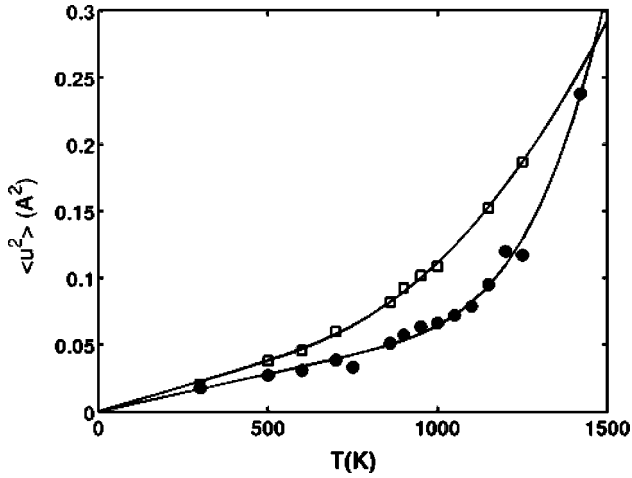
FIG. 7. Mean-square amplitudes of vibration, $\langle u_z^2 \rangle$ (solid circles) and $\langle u_x^2 \rangle$ (squares), for the first layer of the V(111) surface as a function of temperature. The solid lines are a fit to the data.

The in-plane components of the mean-square amplitudes of vibration for the various faces of vanadium are shown in Fig. 8. As may be seen from the figure the in-plane MSVA is largest for the V(111) and smallest for the V(011) surface. Atoms which belong to the loose-packed surface V(111) are less tightly bound than atoms of the close-packed V(011) face and therefore vibrate with larger amplitudes.

### C. Layer density profiles

In order to display the structure of the sample along the $z$ direction, perpendicular to the surface, it is convenient to use the density $\rho(z)$, defined so that $\rho(z)dz$ is the number of atoms in a slice of thickness $dz$ at $z$. We represent $\rho(z)$ by a continuous function defined according to Chen *et al.*:[27,28]

$$\rho(z) = \left\langle \frac{1}{\sqrt{2\pi\Delta z}} \sum_i \exp\left( -\frac{(z-z_i)^2}{2\Delta z} \right) \right\rangle, \qquad (4)$$
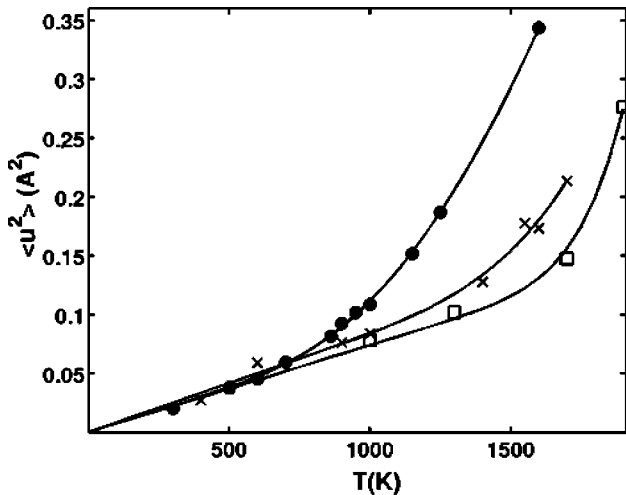


FIG. 8. The calculated in-plane components of mean-square amplitudes of vibration, $\langle u_y^2 \rangle$, for the first surface layer of V(111) (solid circles), V(001) (crosses), and V(011) (squares) as a function of temperature. The solid lines are a fit to the data.
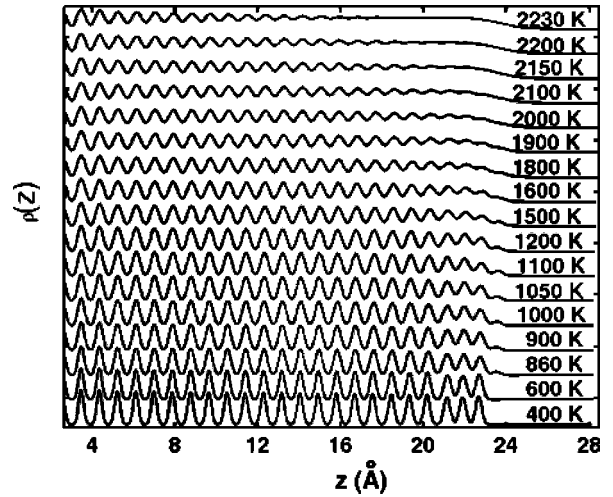


FIG. 9. Density profile across the V(111) slab along the $z$ direction at various temperatures.

where $z_i$ is the $z$ coordinate of atom $i$, with $z=0$ set at the bottom of the first layer which is not fixed, and the angular brackets indicate a time average. The width of each slice, $\Delta z$, is chosen as a trade-off between high contrast and low noise. A small $\Delta z$ results in too few particles in each slice, which leads to large statistical errors (noise). A large $\Delta z$ averages out the density variations (low contrast). Our choice of $\Delta z = 0.1 a_0 / 2\sqrt{3}$, although arbitrary, appears to satisfy both requirements reasonably well.

For a system in equilibrium, $\rho(z)$ can be obtained by an average over many different configurations. Plots of $\rho(z)$ at different temperatures are given in Fig. 9 for the V(111) slab, in Fig. 10 for the V(011) slab, and in Fig. 11 for the V(001) slab.

Premelting effects at the crystal surface can be examined by monitoring the layer-by-layer modulation of the density profile of the system, $\rho(z)$, at various temperatures up to the melting point $T_m$. At low temperatures $\rho(z)$ consists of a
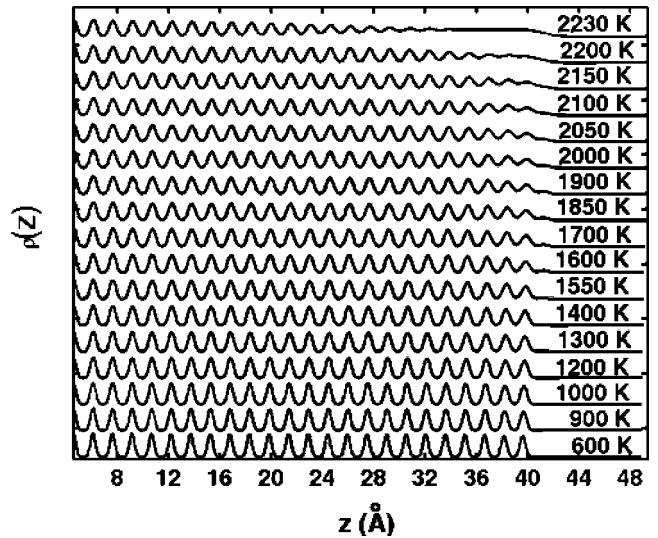


FIG. 10. Density profile across the V(001) slab along the $z$ direction at various temperatures.
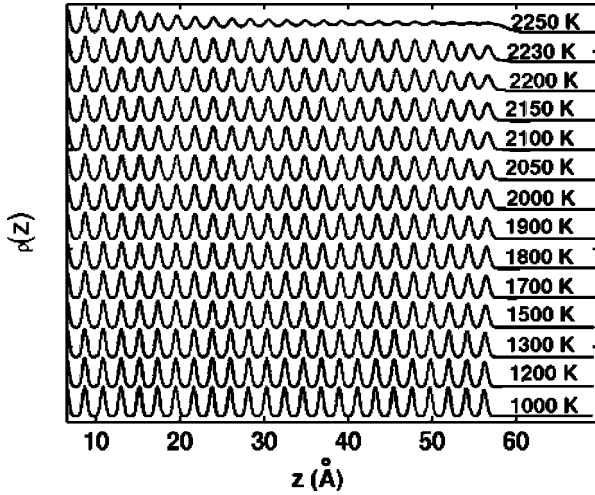
FIG. 11. Density profile across the V(011) slab along the $z$ direction at various temperatures.



FIG. 12. In-plane structure factor $\eta_x$ of the V(111) slab along the $x$ direction vs layer number at several temperatures: $T=400$ K (circles), $T=860$ K (squares), $T=1100$ K (diamonds), $T=1500$ K (down triangles), $T=1800$ K (up triangles), $T=2100$ K (left triangles), $T=2200$ K (right triangles), and $T=2230$ K (crosses).

series of well-resolved peaks. The atoms are packed in the layers with constant density in each layer and virtually no atoms in between these layers. As the temperature increases the effective width of each layer becomes broader due to the enhanced atomic vibration. The position of the density peaks moves to larger values of $z$ due to the thermal expansion. At higher temperatures the atomic vibration becomes so large, especially in the topmost layers, that the minima of $\rho(z)$ in between two layers rise to nonzero values. In addition, disorder sets in, with atomic migration taking place between the layers. Comparing Figs. 9 and 10, one can see that the V(111) surface crosses over to a state of premelting first, then V(001), while on the V(011) surface premelting effects are very small.

Above some temperature [$T_{pm} \simeq 1000$ K for the V(111) surface, $T_{pm} \simeq 1800$ K for the V(001) surface, $T_{pm} \simeq 2200$ K for the V(011) surface] the density of the topmost layer becomes slightly lower than that of the underlying layers. This loss of density is compensated by the appearance of an adlayer. The adlayer appears first on the least-packed surface V(111) and then at a higher temperature on the V(001) surface. The close-packed face V(011) develops an adlayer at temperatures very close to $T_m$. This hierarchy indicates that the formation energy of structural defects (vacancy-adatom pairs) is different on these surfaces. That hierarchy was also observed in the investigation of the surface premelting of fcc metals [Al (Refs. 30 and 40), Ni (Refs. 26–29), and Cu (Refs. 17 and 27)], where it was found that an adlayer appears first on the least-packed (011) surface, then at higher temperature on the (001) face, and finally on the close-packed (111) surface at a temperature close to $T_m$. As the temperature increases towards $T_m$ the distinction between the surface layers becomes blurred. These layers resemble a liquid as far as the density, radial distribution function, diffusion coefficients, etc. On the other hand, some crystalline order is still evident—for example, the anisotropy of these properties. Hence, the term quasiliquid is used to describe these layers.
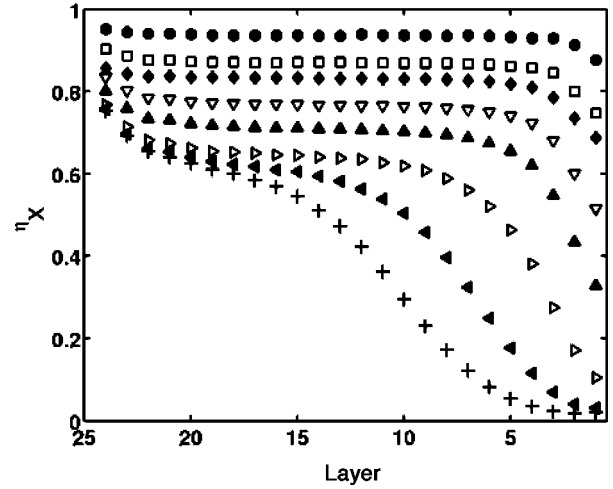
### D. Layer structure factors

The preceding section dealt with the onset of disorder along the $z$ direction, perpendicular to the surface. In order to monitor the onset of in-plane disorder in each atomic layer, it is useful to define a structure factor (order parameter) $\eta_{l,\alpha}$ through a Fourier transform of the atomic density which is calculated separately for each layer:

$$\eta_{l,\alpha} = \left\langle \frac{1}{n_l^2} \left| \sum_{j \in l} \exp(i \vec{g}_\alpha \vec{r}_j) \right|^2 \right\rangle, \qquad (5)$$

where $\alpha = x,y$ and $\vec{g}_\alpha = 2\pi/a_\alpha \vec{e}_\alpha$ is a set of reciprocal lattice vectors. $a_\alpha$ is the distance between nearest neighbors, and $n_l$ is the instantaneous number of atoms in the layer $l$. The sum extends over particles in the layer $l$, and the angular brackets denote averaging over time.

For an ordered crystalline surface the structure factor is a unity at zero temperature. Enhanced vibration and formation of point defects lead to a decrease of the structure factor with increasing temperature. This is illustrated in Figs. 12 and 13 where the structure factor along the $x$ direction is plotted versus layer number for the V(111) and V(011) slabs, respectively. It is seen that these effects are most pronounced in the surface region. Vacancies do not directly affect the order parameter, since a normalization procedure is employed during each measurement by using the instantaneous layer occupation $n_l$ of a layer. Nevertheless, vacancies have an indirect effect on the order parameter by introducing a localized lattice distortion.

As Figs. 12 and 13 show, for the V(111) slab we found a continuous decrease of the in-plane order parameter. In contrast, the close-packed V(011) sample exhibits a relatively abrupt decrease of the structure factor within less than $\sim 20$ K of the melting temperature.
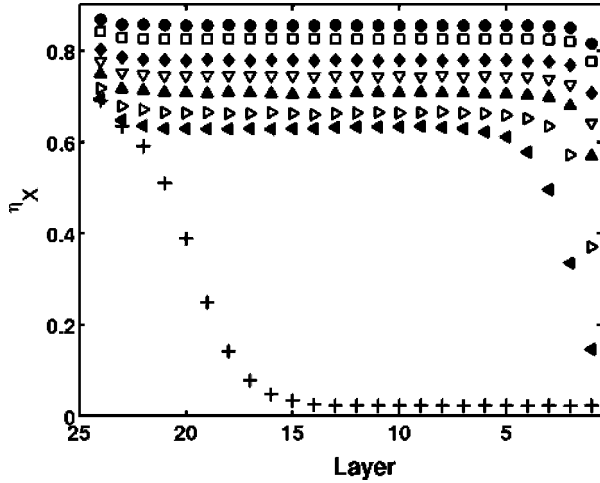
FIG. 13. In-plane structure factor $\eta_x$ of the V(011) slab calculated along the $x$ direction vs layer number at several temperatures: $T=1000$ K (circles), $T=1200$ K (squares), $T=1500$ K (diamonds), $T=1700$ K (down triangles), $T=1900$ K (up triangles), $T=2100$ K (left triangles), $T=2230$ K (right triangles), and $T=2250$ K (crosses).

### E. Radial distribution function

The formation of a quasiliquid film can be analyzed by using a plane radial distribution function defined as

$$p_l(r_{||}) = \left\langle \frac{1}{n_l} \sum_{i,j\in l} \frac{\delta(r_{ij,||}-r_{||})}{2\pi r_{||}} \right\rangle, \quad (6)$$

where $r_{ij,||}$ is the component of the $\vec{r}_i - \vec{r}_j$ parallel to the surface plane, $n_l$ is the instantaneous number of atoms in layer $l$, the sum extends over all particles in layer $l$, and the angular brackets denote averaging over time.

The two-dimensional radial distribution function $p(r_{||})$ for several layers of the V(111) and V(011) slabs very close to $T_m$ is shown in Figs. 14 and 15. As seen from the figures
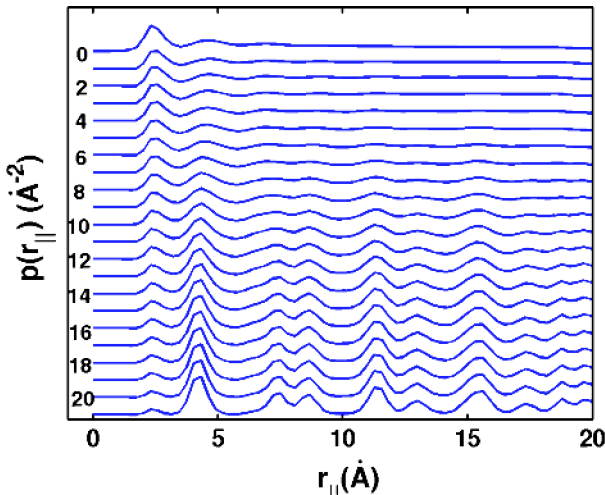


FIG. 14. Two-dimensional radial distribution function $p(r_{||})$ of the top surface layers of V(111) at temperature $T=2230$ K. The layer $n=0$ corresponds to the adlayer, $n=1$ to the first layer, $n=2$ to the second one, etc.
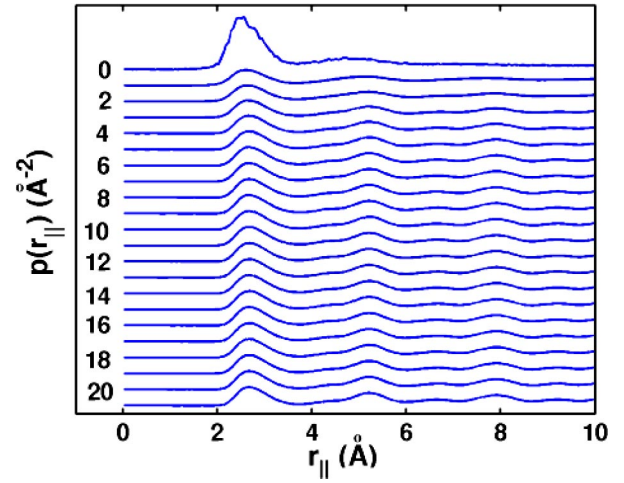


FIG. 15. Two-dimensional radial distribution function $p(r_{||})$ of the surface layers of V(011) at temperature $T=2230$ K. The layer $n=0$ corresponds to the adlayer, $n=1$ to the first layer, $n=2$ to the second one, etc.

the intralayer structure in these layers changes gradually from crystalline to liquid like as one approaches the surface. Particularly noticeable is the disappearance of the crystalline features in $p(r_{||})$ that correspond to the second, third, and other nearest neighbors. In addition to the heights of the peaks, the area under the $p(r_{||})$ curve changes, which reflects the change in the density across the solid-liquid interface.

The plane pair-correlation functions for the first layer of the V(001) at elevated temperatures are shown in Fig. 16. It is clear that the crystalline structure vanishes gradually and the layer becomes quasiliquid as the melting point $T_m$ is approached.

We conclude from the analysis of the plane radial distribution functions and density profiles that surface premelting begins first on the least-packed surface V(111), while changes only appear on the closed-packed V(011) surface at temperatures which are very close to the melting point.
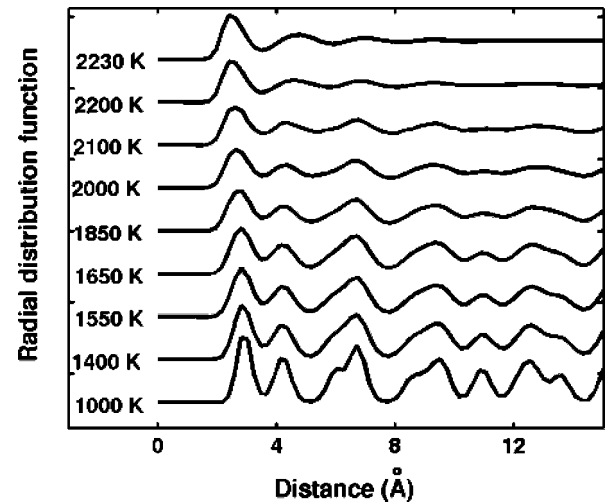


FIG. 16. Two-dimensional radial distribution function $p(r_{||})$ of the first layer of V(001) at various temperatures.
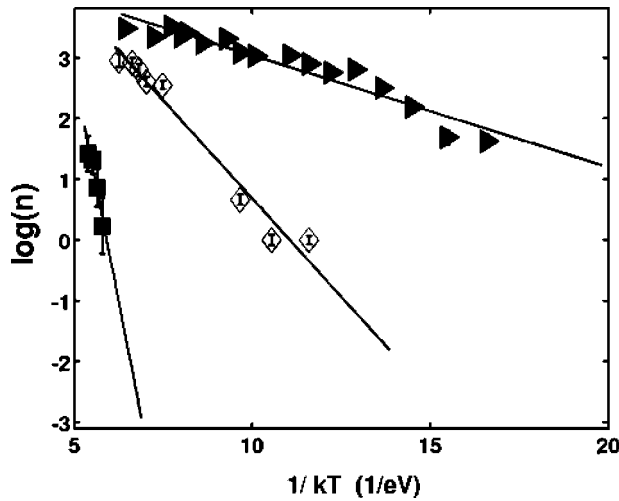
FIG. 17. The natural logarithm of the equilibrium adatom concentration $n$ as a function of $1/k_b T$ on the V(001), V(011), and V(111) faces (denoted by diamonds, triangles, and squares, respectively.) The dashed lines are linear fits to the data.

### F. Layer occupation and point defects

As seen in the density profiles (Figs. 9–11), the formation of an adlayer on the least-packed surface V(111) begins at around $T \sim 800$ K. At these temperatures, the appearance of an adlayer involves the generation of vacancies only in the first surface layer, while at higher temperatures ($T \geq 1600$ K) vacancies in the underlying layers (the second and third layers) begin to appear via promotion of atoms to vacant sites in the first surface layer. Atom migration from the deeper layers into the surface layers increases significantly as the temperature approaches $T_m$. In contrast to the V(111) sample, adlayer formation and generation of adatom-vacancy pairs at the V(001) surface becomes observable only above $T \sim 1400$ K (in practice, all adatoms come from the first layer).

The same effect—namely, the appearance of an adlayer at different surfaces at successively higher temperatures—was observed in computer simulations of surface premelting of fcc metals,[17,24,27,28,30] where the lowest-density (110) surface of fcc metals begins to disorder first, while the close-packed (111) surface preserves its ordered crystalline structure almost up to $T_m$.

Knowledge of the equilibrium-averaged number of atoms in the adlayer allows us to estimate $E_s$, the formation energy of a surface defect (adatom-vacancy pair), according to the relation

$$n/N(T=0) = \exp(-E_s/k_B T), \qquad (7)$$

where $n$ is the adlayer occupation number at a temperature $T$ and $N(T=0)$ is the number of atoms in a layer at zero temperature. Equation (7) holds as long as the surface structure is preserved, and interactions between defects can be neglected. Hence, we used the adlayer occupation data in a temperature region in which the concentration of adatom-vacancy pairs is small. The natural logarithm of adlayer occupation versus $1/k_b T$ is shown in Fig. 17 for the V(111), V(001), and V(011) surfaces, respectively. The calculated

TABLE I. Formation energy $E_s$ of adatom-vacancy pairs. Top line, Eq. (7); second line, Eq. (8). The data for Cu is from Ref. 24. Units are in eV.

| Surface | (111) | (001) | (011) |
|---|---|---|---|
| V (bcc) (eV) | $0.6 \pm 0.2$ | $0.67 \pm 0.03$ | $2.68 \pm 0.2$ |
| V (bcc) (eV) | $0.53 \pm 0.05$ | $0.73 \pm 0.05$ | $2.5 \pm 0.3$ |
| Cu (fcc) (eV) | 1.92 | 0.86 | 0.39 |

surface defect formation energies of the various low-index faces of vanadium are tabulated in Table I.

An alternative method of estimating values of $E_s$ is to use the contribution of defects to anharmonicity, as reflected in the temperature dependence of the mean-square vibration amplitude $\langle u^2 \rangle$. Because the lattice in the vicinity of a defect is distorted, the value of $\langle u^2 \rangle$ will be larger for atoms near a defect. The layer averaged contribution to $\langle u^2 \rangle$ will therefore be proportional to the number of defects, $n$, and hence to $\exp(-E_s/k_B T)$. To extract $E_s$, we have fitted our $\langle u^2 \rangle$ data to the form

$$\langle u^2 \rangle = aT + b(T)\exp(-E_s/k_B T), \qquad (8)$$

where $a$ is a constant and $b(T)$ is a low-order polynomial in $T$. We found that taking $b(T)$ to be first order in $T$—namely, $b(T) = bT$—was sufficient to obtain a good fit. Typical fits were shown as solid lines in Figs. 7 and 8. Values of $E_s$ deduced from these fits for the various surfaces are given in Table I. There is good agreement between the values of $E_s$ obtained by the two methods.

To summarize this subsection, the formation energy of surface defects is lowest at the V(111) surface and increases at the V(001) and V(011) surfaces. This hierarchy is consistent with the results obtained for various faces of copper (fcc lattice) by Häkkinen and Manninen.[24] In both cases, the surface defect formation energy is largest for the close-packed surfaces [V(011) in case of a bcc lattice and Cu(111) in case
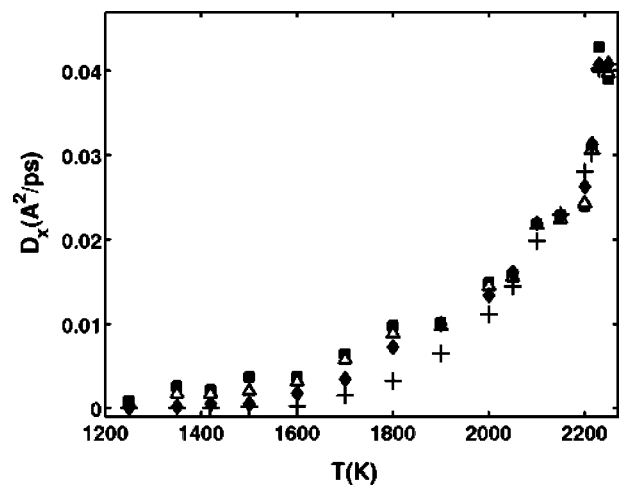


FIG. 18. Diffusion coefficients in layers, vs temperature, for the V(111) system along the $x$ direction ($[1\bar{1}0]$). Squares correspond to the adlayer, $l=0$, triangles to the first layer, $l=1$, diamonds to the second layer, $l=2$, and crosses denote coefficients of diffusion in layer $l=3$.
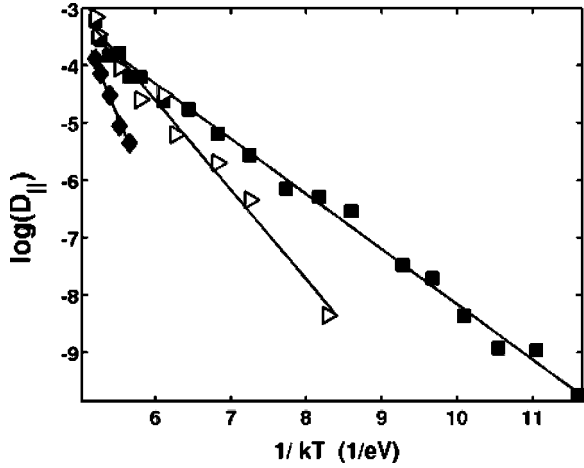
FIG. 19. Plot of natural logarithm of the in-plane diffusion coefficient $\ln(D_{\parallel})$, for the various faces of vanadium as a function of inverse temperature. $(D_{\parallel})$ is in units of $\text{Å}^2/\text{ps}$.

of a fcc lattice] and lowest for the least-packed surfaces V(111) and Cu(011), respectively.

### G. Diffusion coefficients

Mass transport at surfaces can be characterized using the self-diffusion coefficients. These coefficients are found from the particle trajectories $\vec{r}_{i,\mu}(t)$ by calculating the average mean-square displacement $R^2_{l,\mu}$:

$$R^2_{l,\mu} = \left\langle \frac{1}{n_l} \sum_{i \in l} [\vec{r}_{i,\mu}(t+\tau) - \vec{r}_{i,\mu}(\tau)]^2 \right\rangle, \qquad (9)$$

where $\mu = x, y, z$ is a coordinate index, the sum includes atoms in the layer $l$, and the angular brackets denote averaging over time from the origin ($\tau$).

The diffusion coefficients $D_{l,\mu}$ are calculated separately for each layer in the $x$, $y$, and $z$ directions, according to the Einstein relation

$$D_{l,\mu} = \lim_{t \to \infty} \frac{R^2_{l,\mu}}{2t}. \qquad (10)$$

Values of the diffusion coefficients versus layer number are shown in Fig. 18. As expected, the mobility of atoms is larger the closer one comes to the surface. At high enough temperatures, where the surface layers become quasiliquid, the diffusion coefficient is the same (within the error bars) for all the atoms in the region of the surface. These observations correlate with the structural variations in the surface region exhibited in the pair correlation functions, the structure order parameters, and local density profiles.

The natural logarithm of the in-plane diffusion coefficients $D_{\parallel} = \frac{1}{2}(D_x + D_y)$ for the first surface layer of the various faces versus temperature is shown in Fig. 19. Within our accuracy, the diffusion can be characterized by a simple exponential dependence throughout the whole temperature range, $D(T) \propto \exp(-E_d/k_B T)$, with diffusion activation energy $E_d$ being independent of temperature. Values of $E_d$ for

TABLE II. Calculated diffusion activation energy $E_d$ and migration energy $E_m$.

| Surface | V(111) | V(001) | V(011) |
|---|---|---|---|
| $E_d$ (eV) | $0.96 \pm 0.02$ | $1.56 \pm 0.03$ | $3.29 \pm 0.2$ |
| $E_m$ (eV) | $0.43 \pm 0.07$ | $0.87 \pm 0.08$ | $0.79 \pm 0.5$ |

the various low-index faces are given in Table II. The diffusion coefficient of the least packed V(111) face is the largest. The diffusion coefficient of V(001) is smaller, but still larger than the diffusion coefficient of the close packed V(011) surface. In the temperature range where the surface region is still solid like, diffusion takes place mainly by atoms exchanging places with vacancies. Writing $E_d$ as a sum of the formation energy $E_s$ and migration energy $E_m$, and using the values of $E_s$ from the preceding section, we can obtain values of $E_m$ for the various surfaces. These are listed in Table II. It is seen that the migration energy for the V(111) surface is again the lowest, while for the other two surfaces $E_m$ is the same within the error bars of our calculation.

### IV. CONCLUSIONS

In this paper we extended simulations of thermodynamic melting of fcc metals to the bcc structure. This was done in order to compare whether the variety of premelting phenomena in these to structures is similar or not. To this end, we investigated premelting effects at the various surfaces of vanadium using molecular dynamics simulations. We determined the thermodynamic melting temperature of vanadium described by the FS potential as $2220 \pm 10$ K (V(111) surface) and studied structural, transport (diffusion), and energetic properties (formation energy of surface defects).

We found that the surface region of V(111) begins to disorder first, via the generation of vacancy-adatom pairs and the formation of an adlayer at temperatures above 1000 K. At higher temperatures, the surface region becomes quasiliquid. This process begins above 1600 K for the V(001) surface. At the closest-packed V(011) surface, this effect is observed only in close proximity of $T_m$.

The results of our simulations of surface premelting of the bcc metal, vanadium, are similar to the results obtained for various fcc metals, in the sense that the onset of disorder is seen first at the surface with the lowest density.[41]

*Electronic address: phsorkin@techunix.technion.ac.il; URL: http://phycomp.technion.ac.il/ phsorkin/index.html

[1] A. R. Ubbeldone, *Melting and Crystal Structure* (Clarendon, Oxford, 1965).

[2] F. Lindemann, Z. Phys. **11**, 609 (1910).

[3] J.G. Dash, Rev. Mod. Phys. **71**, 1737 (1999).

[4] Y. Ida, Phys. Rev. **187**, 951 (1969).

[5] M. Born, J. Chem. Phys. **7**, 591 (1939).

[6] J.L. Tallon, Philos. Mag. A **39**, 151 (1979).

[7] D. Wolf, P.R. Okamoto, S. Yip, J.F. Lutsko, and M. Kluge, J. Mater. Res. **5**, 286 (1990).

[8] A.V. Granato, Phys. Rev. Lett. **68**, 974 (1992).

[9] T.A. Weber and F.H. Stillinger, J. Chem. Phys. **81**, 5095 (1984).

[10] R.W. Cahn, Nature (London) **413**, 582 (2001).

[11] A. Kanigel, J. Adler, and E. Polturak, Int. J. Mod. Phys. C **12**, 727 (2001).

[12] J.G. Dash, Contemp. Phys. **43**, 427 (2002).

[13] R.W. Cahn, Nature (London) **323**, 668 (1986).

[14] J.W.M. Frenken and J.F. van der Veen, Phys. Rev. Lett. **54**, 134 (1985).

[15] J. F. van der Veen, in *Phase Transitions in Surface Films 2*, edited by H. Taub *et al.* (Plenum, New York, 1991).

[16] A. Trayanov and E. Tosatti, Phys. Rev. B **38**, 6961 (1988).

[17] R.N. Barnett and U. Landman, Phys. Rev. B **44**, 3226 (1991).

[18] S.R. Phillpot, S. Yip, and D. Wolf, Comput. Phys. **3**, 20 (1989).

[19] V. Sorkin, E. Polturak, and Joan Adler, preceding paper, Phys. Rev. B **68**, 174102 (2003).

[20] R. Lipowsky, Phys. Rev. Lett. **49**, 1575 (1982).

[21] R. Lipowsky, U. Breuer, K.C. Prince, and H.P. Bonzel, Phys. Rev. Lett. **62**, 913 (1989).

[22] O. Tomagnini, F. Ercolessi, S. Iarlori, F.D. Di Tolla, and E. Tosatti, Phys. Rev. Lett. **76**, 1118 (1996).

[23] R. Ohnesorge, H. Lowen, and H. Wagner, Phys. Rev. E **50**, 4801 (1994).

[24] H. Hakkinen and M. Manninen, Phys. Rev. B **46**, 1725 (1992).

[25] H. Hakkinen and U. Landman, Phys. Rev. Lett. **71**, 1023 (1993).

[26] Y. Beaudet, L.J. Lewis, and M. Persson, Phys. Rev. B **50**, 12 084 (1994).

[27] E.T. Chen, R.N. Barnett, and U. Landman, Phys. Rev. B **41**, 439 (1990).

[28] E.T. Chen, R.N. Barnett, and U. Landman, Phys. Rev. B **40**, 924 (1989).

[29] H. Cox, R.L. Johnston, and J.N. Murrel, Surf. Sci. **67**, 373 (1996).

[30] P. Stoltze, J.K. Norskov, and U. Landman, Phys. Rev. Lett. **61**, 440 (1988).

[31] J.Q. Broughton, G.H. Gilmer, and K.A. Jackson, Phys. Rev. Lett. **49**, 1496 (1982).

[32] J.Q. Broughton and G.H. Gilmer, J. Chem. Phys. **79**, 5119 (1983).

[33] D. Rapaport, *The Art of MD Simulations* (Cambridge University Press, Cambridge, England, 1991).

[34] M. P. Allen and D. J. Tildesley, *Computer Simulations of Liquids* (Clarendon, Oxford, 1987).

[35] M. Finnis and J. Sinclair, Philos. Mag. A **56**, 11 (1987).

[36] J. Adler, A. Hashibon, N. Schreiber, A. Sorkin, S. Sorkin, and G. Wagner, Comput. Phys. Commun. **12**, 623 (2002).

[37] J. Adler, V. Sorkin, and E. Polturak (unpublished).

[38] J.F. Lutsko, D. Wolf, S.R. Phillpot, and S. Yip, Phys. Rev. B **40**, 2841 (1989).

[39] *Handbook of Chemistry and Physics*, 81st ed., edited by D. R. Lide (CRC Press, Boca Raton, 2001).

[40] P. Stoltze, J. Chem. Phys. **92**, 6306 (1990).

[41] Z.H. Jin, P. Gumbsch, K. Lu, and E. Ma, Phys. Rev. Lett. **87**, 055703 (2001).